УДК 539.3

Аналитический анализ тепловых напряжений в перфорированном симметричном слоистом композите с квазитреугольным отверстием

M.H. Bayati Chaleshtari[1], H. Khoramishad[1], and F. Berto[2]

[1] Научно-технологический университет Ирана, Тегеран, 16846, Иран
[2] Норвежский университет естественных и технических наук, Тронхейм, 7491, Норвегия

В статье изучено распределение тепловых напряжений вокруг квазитреугольного отверстия в симметричном слоистом композите, состоящем из слоев различных композиционных материалов. На основе решения двумерной задачи термоупругости для стационарного случая в рамках метода комплексных переменных аналитически исследовано поведение композита под воздействием однородного теплового потока. Аналитическое решение получено путем преобразования решения Лехницкого с использованием классической теории слоистых пластин и функции конформного отображения. Изучено влияние ряда параметров на распределение тепловых напряжений вокруг отверстия, включая ориентацию отверстия, степень закругления углов и соотношение сторон отверстия, угол теплового потока, последовательность укладки, а также материал слоев. Результаты приведены для различных последовательностей укладки $[45°/–45°]_s$ и $[0°/90°]_s$. Найденное аналитическое решение показывает хорошее соответствие с результатами, полученными методом конечных элементов.

Ключевые слова: метод комплексных переменных, квазитреугольное отверстие, симметричный слоистый композит, тепловое напряжение, последовательность укладки слоев

DOI 10.24411/1683-805X-2020-11008

Analytical thermal stress analysis of perforated symmetric composite laminates containing a quasi-triangular hole

M.H. Bayati Chaleshtari[1], H. Khoramishad[1], and F. Berto[2]

[1] School of Mechanical Engineering, Iran University of Science and Technology, Narmak, Tehran, 16846, Iran
[2] Department of Mechanical and Industrial Engineering, Norwegian University of Science and Technology, Trondheim, 7491, Norway

In this study, the thermal stress distribution surrounding a quasi-triangular hole within a symmetric composite laminate made of various composite materials was investigated. A composite laminate exposed to uniform heat flux was analyzed using the complex variable method as a thermo-elastic two-dimensional problem under a steady state condition. The analytical solution was achieved with the development of the Lekhnitskii's solution and using the classical laminated plate theory and a conformal mapping function. The influence of important parameters on thermal stress distribution surrounding a hole such as the hole orientation, bluntness and aspect ratio, the heat flux angle and the laminate stacking sequence and material was studied. The results were achieved for different stacking sequences of $[45°/–45°]_s$ and $[0°/90°]_s$. The analytical solution in this study was well validated against the finite element results.

Keywords: complex variable method, quasi-triangular hole, symmetric laminated composite, thermal stress, stacking sequence

1. Introduction

Polymeric composites have been adopted as an inevitable class of materials in various industrial sectors such as marine, gas and oil, automotive and aerospace due to their advantages. The advantages of laminated composite materials are well-known such as high corrosion resistance, high impact strength and low structural weight. Holes are usually made in structures for various reasons, for instance to provide manholes as the points of entry and exit or to reduce the weight of structures. It is very likely that a perforated composite laminate is exposed to thermal loads. The holes and cutouts, as geometrical discontinuities can easily disturb the uniform heat flow in structures

giving rise to thermal stresses. These thermal stresses accumulate on the mechanical stresses and can result in structural failure.

2. Literature review

Many researches have studied thermal stress distribution around holes within isotropic and anisotropic plates using different methods. The complex variable technique is an efficient approach to address this class of problems. The complex variable technique has been used by many researchers for solving two-dimensional boundary value problems [1–5]. Bhullar et al. [6] evaluated thermal stresses induced in anisotropic plates containing an elliptical hole using an analytical approach and by considering isothermal state for the hole edges. Tarn and Wang [7] obtained stresses due to thermal loads in an anisotropic elastic plate with a circular hole by applying the Lekhnitskii complex variable technique and by assuming the plane strain and plane stress conditions. Sharma and Chauhan [8] studied stresses induced surrounding a noncircular hole in an anisotropic finite laminate subjected to mechanical loading using the complex variable technique. The parameters such as the plate size and the hole geometry were investigated. Kalyon and Yilbas [9] determined the temperature and thermal stress distributions in a plate under laser pulse heating using a closed-form solution obtained using the Laplace transformation method.

Su et al. [10] studied stress concentration around the triangular and square holes in composite laminates under in-plane tensile loading. They used analytical solution and conformal mapping function to obtained the optimum hole shape. Ju et al. [11] used an analytical solution for obtaining the deformation and stress fields in multilayer composite laminates under mechanical loading. Alshaya and Lin [12] used an analytical solution to determine the stress distribution around a circular hole located in an isotropic plate using the hybrid complex-variable method. Damghani et al. [13] utilized the Lekhnitskii's complex variable method and obtained the stress resultant distribution at the edge of an elliptical or circular hole in an infinite composite plate under membrane loading. Moreover, they studied the effect of composite laminate stiffness on the stress resultant concentration factor around a circular hole.

Khechai and Mohite [14] obtained the optimum fiber and load orientation angles and the hole size in a perforated lamina as well as the symmetric composite plates having circular hole under different in-plane loading conditions using an analytical approach. Jafari et al. [15] employed the Florence and Goodier approach to analyze thermoelastic stresses in an isotropic plate with a polygonal hole under constant heat flux. Furthermore, Jafari and Jafari [16] presented the stress distribution surrounding a noncircular hole within an infinite composite plate under steady state condition by utilizing the two-dimensional thermoelastic theory. Choi [17] analyzed an infinite orthotropic plate containing two parallel cracks subjected to constant heat flux. The presence of insulated cracks disturbed the uniform heat flow. Mahmoudi and Atefi [18] obtained a comprehensive analytical solution for thermal stresses in a hollow cylinder subjected to periodic time-varying thermal loading on the inner surface and by insulating the outer circular surface and maintaining the temperature of the both lateral surfaces constant. They employed the Fourier expansion and general properties of Bessel functions. Chao et al. [19] introduced an analytical solution based on the complex potential technique to assess the stress distribution surrounding multiple circular holes under constant heat flux. Wang et al. [20] analyzed the stress distribution in a perforated plate made of different materials containing a circular cutout using the complex variable technique. Zenkour and Abouelregal [21] studied the interactions between the effective parameters influencing the thermal stress distribution around a perforated cylinder. They applied thermoelasticity method and Laplace solution to derive the solution of the problem. Ukadgaonker and Rao [22] studied symmetric laminates under in-plane loading containing various holes by applying a complex variable technique. Zha and Zuo [23] utilized analytical and experimental methods to investigate the strength and stress distribution in laminates containing holes. They used finite element method to validate the proposed method. Dehghani et al. [24] investigated thermal stresses surrounding triangular and square holes in a finite isotropic plate using analytical solution. They applied conformal mapping function and complex variable technique to obtain the thermal stress value around the hole.

The main purpose of this paper was investigating thermal stresses surrounding a quasi-triangular hole within a symmetric composite laminate using an analytical method. Many researches have analyzed stresses around circular and elliptical holes in metallic plates and few researchers have examined noncircular holes

in symmetric composite laminates under mechanical loading using analytical methods. In this paper, an analytical method was developed for analyzing thermal stresses in perforated symmetric laminates containing a quasi-triangular hole subjected to uniform heat flux. An equivalent thermal conductivity coefficient was defined and thermal stresses around the hole were determined using the Lekhnitskii complex variable method, classical laminate plate theory and conformal mapping. Moreover, the effect of the laminate stacking sequence as an important parameter [25] together with other significant parameters such as the hole orientation, aspect ratio, bluntness and the heat flux angle was investigated on thermal stresses. The composite laminates made of graphite/epoxy (AS/3501), E-glass/epoxy, carbon/epoxy woven and unidirectional carbon/epoxy with two different stacking sequences of $[45°/–45°]_s$ and $[0°/90°]_s$ were studied.

3. Problem definition

A symmetric composite laminate containing a quasi-triangular hole under a remote uniform heat flux q under steady state condition (Fig. 1) was considered in this study. The material behavior of the composite laminate was assumed orthotropic and linear elastic governed by the generalized Hooke's law. The edges of the quasi-triangular hole were considered thermally insulated. The size of the hole was sufficiently small compared to the laminate size, so the laminate can be assumed infinite. As can be seen in Fig. 1, the hole rotation angle indicating the hole orientation with respect to the horizontal axis was denoted by β. The uniform heat flux was disturbed due to the presence of a thermally insulated quasi-triangular hole giving rise to thermal stresses surrounding the hole. The thermal stresses on the hole edges were confined to the tangential component σ_θ because of the hole boundary conditions. The small deformation and plane stress condition were assumed in the study.

4. Analytical solution

According to classical laminate plate theory, the thermal stress vector in a laminated composite can be obtained by the equation [26]

$$\{\sigma\}^T = \frac{1}{H}\sum_{l=1}^{N}[\bar{Q}]^l\{\bar{\alpha}\}^l t_l T, \tag{1}$$

where $\{\sigma\}^T$ is the thermal stress vector, $[\bar{Q}]^l$ is the reduced stiffness matrix corresponding to the lth layer, T is the temperature change, t_l is the thickness of each lamina and $\{\bar{\alpha}\}^l$ is the thermal expansion coefficient of the lth lamina in off-axis coordinate system and its components can be determined using equations

$$\begin{aligned}\bar{\alpha}_x &= \alpha_{11}m^2 + \alpha_{22}n^2,\\ \bar{\alpha}_y &= \alpha_{11}n^2 + \alpha_{22}m^2,\\ \bar{\alpha}_{xy} &= 2mn(\alpha_{11} - \alpha_{22}),\end{aligned} \tag{2}$$

where α_{11} and α_{22} are the coefficients of thermal expansion in on-axis coordinate system. Moreover, m and n are cosine and sine of the fiber angle γ, respectively. Equation (1) can be simplified as

$$\{\sigma\}^T = \{\Omega\}\cdot T \tag{3}$$

in which

$$\begin{Bmatrix}\Omega_x\\ \Omega_y\\ \Omega_{xy}\end{Bmatrix} = \frac{1}{H}\sum_{l=1}^{N}\begin{bmatrix}\bar{Q}_{11} & \bar{Q}_{12} & \bar{Q}_{16}\\ \bar{Q}_{12} & \bar{Q}_{22} & \bar{Q}_{26}\\ \bar{Q}_{16} & \bar{Q}_{26} & \bar{Q}_{66}\end{bmatrix}^l\begin{Bmatrix}\bar{\alpha}_x\\ \bar{\alpha}_y\\ \bar{\alpha}_{xy}\end{Bmatrix}^l (z_l - z_{l-1}). \tag{4}$$

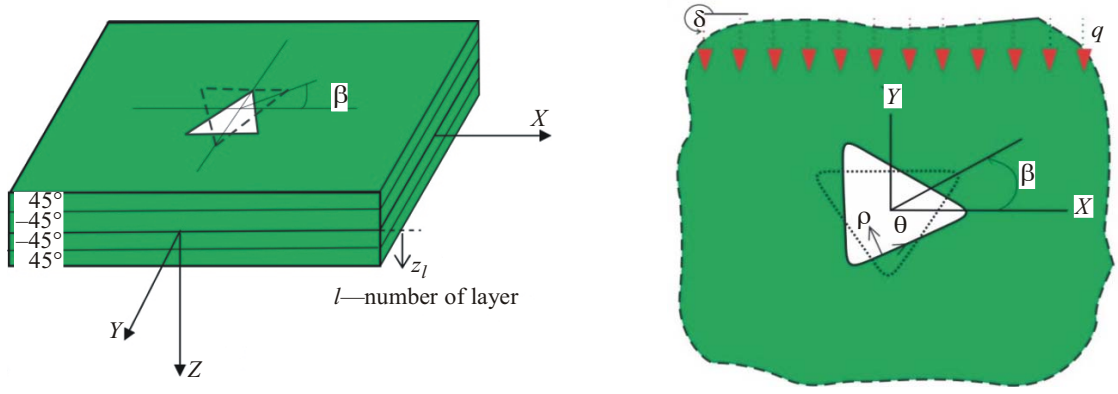

Fig. 1. Symmetric composite laminate containing a quasi-triangular hole under a remote uniform heat flux (color online)

According to the Lekhnitskii's complex potential method and by considering the Airy's stress function $U(x, y)$, the stress components are defined as

$$\sigma_x = \frac{\partial^2 U}{\partial y^2},\ \sigma_y = \frac{\partial^2 U}{\partial x^2},\ \tau_{xy} = -\frac{\partial^2 U}{\partial x \partial y}. \tag{5}$$

The compatibility equation for a planar geometry is presented as

$$\frac{\partial^2 \varepsilon_x^0}{\partial y^2} + \frac{\partial^2 \varepsilon_y^0}{\partial x^2} = \frac{\partial^2 \gamma_{xy}^0}{\partial x \partial y}. \tag{6}$$

Combining Eq. (5), the compatibility equation and the stress-strain relations gives the compatibility equation of an anisotropic material in terms of the stress function [3]:

$$a_{11}\frac{\partial^4 U}{\partial y^4} - 2a_{16}\frac{\partial^4 U}{\partial x \partial y^3} + (2a_{12} + a_{66})\frac{\partial^4 U}{\partial x^2 \partial y^2} - 2a_{26}\frac{\partial^4 U}{\partial x^3 \partial y} + a_{22}\frac{\partial^4 U}{\partial x^4} = -\alpha_x \frac{\partial^2 T}{\partial y^2} + \alpha_{xy}\frac{\partial^2 T}{\partial x \partial y} - \alpha_y \frac{\partial^2 T}{\partial x^2}. \tag{7}$$

In Eq. (7), a_{ij} are the coefficients of the reduced compliance matrix of the symmetric laminate and α_x, α_y and α_{xy} are the thermal expansion coefficients in the global coordinate system and can be obtained as Eq. (8). For simplicity, the overall thickness of the laminate was considered unity:

$$\begin{aligned} \alpha_x &= a_{11}\Omega_x + a_{12}\Omega_y + a_{16}\Omega_{xy}, \\ \alpha_y &= a_{12}\Omega_x + a_{22}\Omega_y + a_{26}\Omega_{xy}, \\ \alpha_{xy} &= a_{16}\Omega_x + a_{26}\Omega_y + a_{66}\Omega_{xy}. \end{aligned} \tag{8}$$

The general solution of Eq. (7) can be considered as the summation of the homogeneous U^{h} and particular U^{p} parts:

$$U = U^{\mathrm{h}} + U^{\mathrm{p}}. \tag{9}$$

The homogeneous form of Eq. (7) can be presented as

$$a_{11}\frac{\partial^4 U^{\mathrm{h}}}{\partial y^4} - 2a_{16}\frac{\partial^4 U^{\mathrm{h}}}{\partial x \partial y^3} + (2a_{12} + a_{66})\frac{\partial^4 U^{\mathrm{h}}}{\partial x^2 \partial y^2} - 2a_{26}\frac{\partial^4 U^{\mathrm{h}}}{\partial x^3 \partial y} + a_{22}\frac{\partial^4 U^{\mathrm{h}}}{\partial x^4} = 0. \tag{10}$$

According to the Lekhnitskii's method, by introducing the four linear first-order differential operators D_k, Eq. (10) can be expressed as [3]

$$D_1 D_2 D_3 D_4 U^{\mathrm{h}} = 0,\ D_k = \frac{\partial}{\partial y} - \mu_k \frac{\partial}{\partial x}, \tag{11}$$

in which μ_k ($k = 1, 2, 3, 4$) are the roots of the characteristic equation

$$a_{11}\mu^4 - 2a_{16}\mu^3 + (2a_{12} + a_{66})\mu^2 - 2a_{26}\mu + a_{22} = 0. \tag{12}$$

The roots of Eq. (12) can be presented as

$$\begin{aligned} &\mu_1 = \alpha_1 + i\beta_1,\ \mu_2 = \bar{\mu}_1 = \alpha_1 - i\beta_1, \\ &\mu_3 = \alpha_2 + i\beta_2,\ \mu_4 = \bar{\mu}_3 = \alpha_2 - i\beta_2, \end{aligned} \tag{13}$$

where α_1, α_2 and β_2 are real numbers. For a symmetric laminate $a_{16} = a_{26} = 0$, so the characteristic equation is reduced to

$$a_{11}\mu^4 + (2a_{12} + a_{66})\mu^2 + a_{22} = 0. \tag{14}$$

The function U^{h} is considered as

$$U^{\mathrm{h}} = 2\,\mathrm{Re}\sum_{k=1}^{2} U_k(Z_k), \tag{15}$$

where Z_k is the mapping function and is defined as

$$Z_k = x + \mu_k y,\ k = 1, 2. \tag{16}$$

By substituting Eq. (15) into Eq. (10) and considering Z_k, function U^{h} is derived. Then Eq. (9) can be rephrased as

$$U = U_1(Z_1) + U_2(Z_2) + \overline{U_1(Z_1)} + \overline{U_2(Z_2)} + U^{\mathrm{p}}. \tag{17}$$

The new stress function ψ is derived from the stress function U in the form

$$\frac{\mathrm{d}U}{\mathrm{d}z} = \psi_1(Z_1) + \psi_2(Z_2) + \overline{\psi_1(Z_1)} + \overline{\psi_2(Z_2)} + \psi^{\mathrm{p}}. \tag{18}$$

By substituting Eqs. (17) and (18) into Eq. (5), the stress components are determined as

$$\begin{aligned} \sigma_x &= 2\,\mathrm{Re}\{\mu_1^2\psi_1'(Z_1) + \mu_2^2\psi_2'(Z_2)\} + \frac{\partial^2 U^{\mathrm{p}}}{\partial y^2}, \\ \sigma_y &= 2\,\mathrm{Re}\{\psi_1'(Z_1) + \psi_2'(Z_2)\} + \frac{\partial^2 U^{\mathrm{p}}}{\partial x^2}, \\ \tau_{xy} &= -2\,\mathrm{Re}\{\mu_1\psi_1'(Z_1) + \mu_2\psi_2'(Z_2)\} - \frac{\partial^2 U^{\mathrm{p}}}{\partial x \partial y}, \end{aligned} \tag{19}$$

in which $\psi_1'(Z_1)$ and $\psi_2'(Z_2)$ are the derivatives of functions $\psi_1(Z_1)$ and $\psi_2(Z_2)$ with respect to Z_1 and Z_2, respectively. The Fourier's law was employed in order to relate the on-axis heat flux q and temperature gradient in a lamina as seen in Eq. (20) [27]:

$$\begin{Bmatrix} q_1 \\ q_2 \\ q_3 \end{Bmatrix} = -\begin{bmatrix} k_{11} & 0 & 0 \\ 0 & k_{22} & 0 \\ 0 & 0 & k_{33} \end{bmatrix} \begin{Bmatrix} \dfrac{\partial T}{\partial x_1} \\ \dfrac{\partial T}{\partial x_2} \\ \dfrac{\partial T}{\partial x_3} \end{Bmatrix}. \quad (20)$$

In Eq. (20), $[k]$ is the on-axis anisotropic thermal conductivity matrix and T is the temperature change. It was assumed that the unidirectional laminae were transversely isotropic (i.e. isotropic in a plane normal to the fibers). Using the transformation matrix, Eq. (20) can be rewritten based on the off-axis coordinate as follows:

$$\left[T(\gamma)\right]\{q\}_{\text{off}} = -k_{\text{on}}\left[T(\gamma)\right]\nabla T_{\text{off}}, \quad (21)$$

where $[T(\gamma)]$ is the inverse of the transformation matrix ($[T(-\gamma)]$) defined in Eq. (22):

$$\left[T(-\gamma)\right] = \begin{bmatrix} \cos\gamma & -\sin\gamma & 0 \\ \sin\gamma & \cos\gamma & 0 \\ 0 & 0 & 1 \end{bmatrix}. \quad (22)$$

Therefore, the Fourier's law of thermal conduction in the global coordinate system can be presented as

$$\{q\}_{\text{off}} = -k_{\text{off}}\nabla T_{\text{off}}. \quad (23)$$

As a result, the off-axis thermal conductivity matrix can be obtained using the equation

$$k_{\text{off}} = \left[T(-\gamma)\right]k_{\text{on}}\left[T(\gamma)\right]. \quad (24)$$

By considering $n = \sin\gamma$ and $m = \cos\gamma$, the components of the off-axis thermal conductivity matrix $k_{\text{off}} = [\bar{k}]$ are defined as

$$\begin{aligned} &\bar{k}_{11} = m^2k_{11} + n^2k_{22},\ \bar{k}_{33} = k_{33}, \\ &\bar{k}_{22} = n^2k_{11} + m^2k_{22},\ \bar{k}_{13} = \bar{k}_{23} = 0, \\ &\bar{k}_{12} = -mn(k_{11} - k_{22}). \end{aligned} \quad (25)$$

The resultant of thermal conductivity coefficients for the laminate can be determined by integrating the off-axis thermal conductivity coefficients across the laminate thickness using the equation

$$[K] = \frac{1}{H}\int_{-H/2}^{H/2}[\bar{k}]^l\,\mathrm{d}t. \quad (26)$$

Equation (26) can be converted into the summation form:

$$\left[K\right] = \frac{1}{H}\sum_{l=1}^{N}[\bar{k}]^l t_l. \quad (27)$$

In Eq. (27), l is the layer number and $[K]$ is the thermal conductivity resultant matrix of the laminate. Due to the stationary heat flow in the laminate, Eq. (28) should be considered:

$$\nabla.q_i = 0\ (i = x, y, z). \quad (28)$$

By substituting Eq. (23) into Eq. (28), the governing equation for temperature is expressed as

$$K_x\frac{\partial^2 T}{\partial x^2} + 2K_{xy}\frac{\partial^2 T}{\partial x\partial y} + K_y\frac{\partial^2 T}{\partial y^2} = 0. \quad (29)$$

A harmonic function of $T(x, y)$ satisfying Eq. (29) can be obtained as the temperature distribution in laminate. The solution of Eq. (29) can be considered as $T = U_t(x + \mu_t y)$ in which μ_t are the roots of the characteristic equation

$$K_y\mu_t^2 + 2K_{xy}\mu_t + K_x = 0. \quad (30)$$

As the thermal conductivity matrix is invertible and positive definite ($K_xK_y > K_{xy}^2$), the characteristic equation (Eq. (30)) contains two complex conjugate roots. Hence, the general solution of Eq. (29) can be considered as [7]

$$\begin{aligned} &T = U_t(Z_t) + \overline{U_t(Z_t)} = 2\,\mathrm{Re}(U_t(Z_t)), \\ &Z_t = x + \mu_t y, \end{aligned} \quad (31)$$

in which U_t is a complex function. By substituting Eq. (31) into Eq. (7), the particular solution for the stress function U can be obtained as

$$U^{\text{p}} = 2\,\mathrm{Re}(\eta U_t(Z_t)), \quad (32)$$

where

$$\begin{aligned} \eta = {} & (-\alpha_y + \alpha_{xy}\mu_t - \alpha_x\mu_t^2)\times \\ & \times(a_{11}\mu_t^4 - 2a_{16}\mu_t^3 + (2a_{12} + a_{66})\mu_t^2 - \\ & - 2a_{26}\mu_t + a_{22})^{-1}. \end{aligned} \quad (33)$$

Moreover, by substituting Eq. (32) into Eq. (19), the stress components and displacement field can be attained in the form of stress functions as

$$\begin{aligned} \sigma_x = {} & 2\,\mathrm{Re}\{\mu_1^2\psi_1'(Z_1) + \mu_2^2\psi_2'(Z_2)\} + \\ & + 2\,\mathrm{Re}(\eta\mu_t^2\psi_t'), \\ \sigma_y = {} & 2\,\mathrm{Re}\{\psi_1'(Z_1) + \psi_2'(Z_2)\} + 2\,\mathrm{Re}(\eta\psi_t'), \\ \tau_{xy} = {} & -2\,\mathrm{Re}\{\mu_1\psi_1'(Z_1) + \mu_2\psi_2'(Z_2)\} - \\ & - 2\,\mathrm{Re}(\eta\mu_t\psi_t'), \\ u_x = {} & 2\,\mathrm{Re}\sum_{k=1}^{2}p_k\psi_k + 2\,\mathrm{Re}(p_t\psi_t), \\ u_y = {} & 2\,\mathrm{Re}\sum_{k=1}^{2}q_k\psi_k + 2\,\mathrm{Re}(q_t\psi_t), \end{aligned} \quad (34)$$

where

$$\begin{aligned} &p_k = a_{11}\mu_k{}^2 + a_{12} - a_{16}\mu_k,\ k = 1, 2, \\ &p_t = \eta(a_{11}\mu_t{}^2 + a_{12} - a_{16}\mu_t) + a_x, \end{aligned} \quad (35)$$

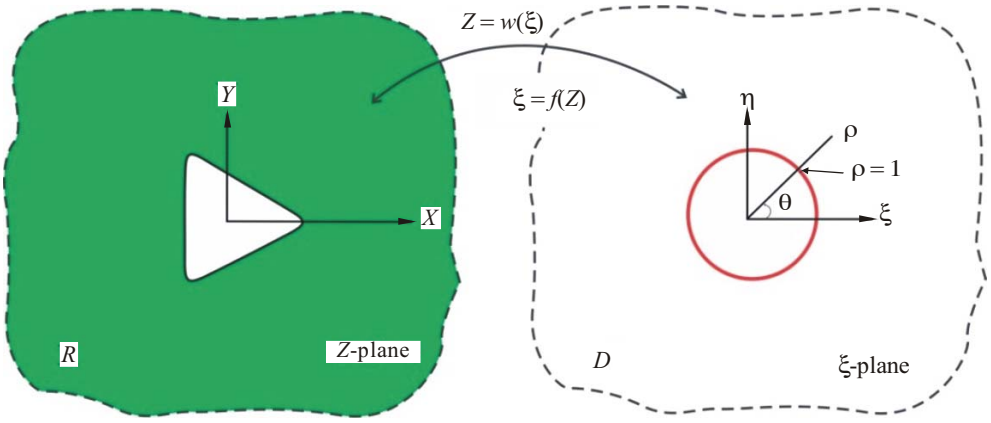

Fig. 2. Conformal mapping (color online)

$$q_k = a_{12}\mu_k + \frac{a_{22}}{\mu_k} - a_{26},\ k = 1, 2,$$
$$q_t = \eta\left(a_{12}\mu_t + \frac{a_{22}}{\mu_t} - a_{26}\right) + \frac{a_y}{\mu_t}.$$

4.1. Conformal mapping

The infinite area outside the quasi-triangular hole was transfer into the outside region of a unit circle to develop the analytical solution of a circular hole into a quasi-triangular hole and to facilitate the application of Cauchy integral equation, as can be seen in Fig. 2.

Equation (36) was used in order to define the mapping function:

$$z_k = w(x) = x + \mu_k y,\ k = 1, 2, t, \tag{36}$$

such that x and y represent the Cartesian coordinates within a laminate with a quasi-triangular hole and can be represented in terms of θ as follows [28]:

$$x = \lambda(\cos\theta + w\cos(2\theta)),$$
$$y = \lambda(c\sin\theta - w\sin(2\theta)). \tag{37}$$

Moreover, in Eq. (36), μ_k are the characteristic equation roots of an anisotropic material as defined in Eq. (13) and ξ, within the mapped plane, is defined in the equation

$$\xi = \rho e^{i\theta} = \rho(\cos\theta + i\sin\theta). \tag{38}$$

For a unit circle ρ = 1. In Eq. (37), c controls the hole elongation in y-direction and w is the bluntness parameter that determines the hole corners curvature. Figure 3 illustrates the influence of the parameter w on the hole shape.

Based on Eqs. (37) and (38), the conformal mapping function for a quasi-triangular hole is obtained as

$$z_k = w(\xi) = \lambda/2\,(\Delta_{1k}\xi + \Delta_{2k}\xi^{-1} + \Delta_{3k}\xi^2 + \Delta_{4k}\xi^{-2}), \tag{39}$$

in which Δ_{ik}, i = 1, 2, 3, 4 are as below:

$$\begin{aligned}
\Delta_{1k} &= \frac{\lambda}{2}[(1 - ic\mu_k)\cos\beta - (ic + \mu_k)\sin\beta],\\
\Delta_{2k} &= \frac{\lambda}{2}[(1 + ic\mu_k)\cos\beta + (ic - \mu_k)\sin\beta],\\
\Delta_{3k} &= \frac{\lambda w}{2}[(1 + i\mu_k)\cos\beta + (i - \mu_k)\sin\beta],\\
\Delta_{4k} &= \frac{\lambda w}{2}[(1 - i\mu_k)\cos\beta - (i + \mu_k)\sin\beta].
\end{aligned} \tag{40}$$

Equation (41) can be applied to model the hole rotation

$$\begin{Bmatrix} X \\ Y \end{Bmatrix} = \begin{bmatrix} \cos\beta & \sin\beta \\ -\sin\beta & \cos\beta \end{bmatrix} \begin{Bmatrix} x \\ y \end{Bmatrix}, \tag{41}$$

in which β is the hole rotation angle, and x and y were defined in Eq. (37).

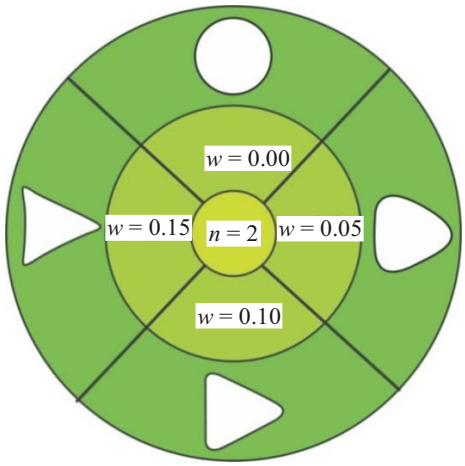

Fig. 3. Effect of the parameter w on the hole shape

4.2. Determination of the complex analytical functions ψ *and* ψ_t

Based on Eq. (34), to achieve the stress components, the complex analytical functions ψ and ψ_t need to be determined. For convenience in formulations, some matrices are defined in equations

$$L=\begin{bmatrix}-\mu_1 & -\mu_2\\ 1 & 1\end{bmatrix},\ l=\begin{bmatrix}-\eta\mu_t\\ \eta\end{bmatrix},$$
$$\psi=\begin{bmatrix}\psi_1\\ \psi_2\end{bmatrix},\ a=\begin{bmatrix}p_t\\ q_t\end{bmatrix},\ A^{\wp}=\begin{bmatrix}p_1 & p_2\\ q_1 & q_2\end{bmatrix}. \tag{42}$$

The triangular hole boundary is not subjected to external loading, thus Eq. (42) is used to rewrite the mechanical boundary conditions as

$$L\psi+\overline{L\psi}+l\psi_t+\overline{l\psi_t}=0. \tag{43}$$

Moreover, as the boundary of the quasi-triangular hole is insulated, the Neumann boundary condition is also considered as

$$\psi_t'(\xi)-\overline{\psi_t'(\xi)}=0. \tag{44}$$

The function $\psi_t'(\xi)$ can be presented by two functions $f_t(\xi)$ and $g_t(\xi)$ (see Eq. (45)) that are holomorphic in the inner and outer areas of the unit circle, respectively [7]:

$$\psi_t'(\xi)=f_t(\xi)+g_t(\xi). \tag{45}$$

By considering the points on the hole boundary ($\xi=\sigma$) and substituting Eq. (45) into Eq. (44) and multiplying it by $d\sigma/(2\pi i(\sigma-\xi))$ and applying the Cauchy integral, $\psi_t'(\xi)$ can be rephrased as

$$\psi_t'(\xi)=f_t(\xi)+\overline{f_t}(\xi^{-1}). \tag{46}$$

The function $\psi_t'(\xi)$ can be expressed as the Laurent series in which the term of ξ^{-1} exists. Subsequently, by integrating $\psi_t'(\xi)$, the function of $\psi_t(\xi)$ contains $\log\xi$:

$$\psi_t(\xi)=F_t(\xi)+G_t(\xi)+\Gamma\log\xi, \tag{47}$$

in which $F_t(\xi)$ and $G_t(\xi)$ are the holomorphic functions inside and outside the unit circle, respectively. Moreover, the function of $\psi(\xi)$ can be considered as [29]

$$\psi(\xi)=f(\xi)+g(\xi)+h\log\xi, \tag{48}$$

where $f(\xi)$ and $g(\xi)$ are holomorphic inside and outside the unit circle, respectively. By substituting Eqs. (47) and (48) into Eq. (43) and multiplying it by $d\sigma/(2\pi i(\sigma-\xi))$ and applying the Cauchy integral, $\psi(\xi)$ can be rewrited as

$$\psi(\xi)=f(\xi)-L^{-1}\overline{L}\,\overline{f}(\xi^{-1})-L^{-1}lG_t(\xi)-L^{-1}\overline{l}\,\overline{F}_t(\xi^{-1})+h\log\xi, \tag{49}$$

where

$$h=L^{-1}(\overline{B}-B)^{-1}(\Gamma a-\overline{\Gamma a})+A^{\wp-1}(\overline{B}^{-1}-B^{-1})^{-1}(\Gamma l-\overline{\Gamma l}),\qquad B=A^{\wp}L^{-1}, \tag{50}$$

in which L and $A^{\wp}$ were defined in Eq. (42), and Γ should be calculated by the application of boundary conditions. When the heat flux is applied to an anisotropic laminate without hole, the thermal stress function can be obtained as [7]

$$\psi_t'^{\infty}=\kappa Z_t, \tag{51}$$

where

$$\kappa=\frac{q(\cos\delta+\bar{\mu}_t\sin\delta)}{K_t(\mu_t-\bar{\mu}_t)},\qquad K_t=i(K_xK_y-K_{xy}^2)^{1/2}. \tag{52}$$

However, in the presence of a quasi-triangular hole, in addition to $\psi_t'^{\infty}$, the function of $\psi_t'^{M}$, which is holomorphic outside the unit circle, should be added to the thermal stress function. Therefore, $\psi_t'(\xi)$ is derived as

$$\psi_t'(\xi)=\kappa(\Delta_{1t}\xi+\Delta_{2t}\xi^{-1}+\Delta_{3t}\xi^2+\Delta_{4t}\xi^{-2})+\psi_t'^{M}(\xi). \tag{53}$$

By comparing Eq. (53) and Eq. (46), the function $f_t(\zeta)$ can be obtained as Eq. (54), so $\psi_t'(\xi)$ can be rewritten as Eq. (55):

$$f_t(\xi)=\kappa\Delta_{1t}\xi+\kappa\Delta_{3t}\xi^2, \tag{54}$$
$$\psi_t'(\xi)=\kappa\Delta_{1t}\xi+\overline{\kappa\Delta_{1t}}\xi^{-1}+\kappa\Delta_{3t}\xi^2+\overline{\kappa\Delta_{3t}}\xi^{-2}. \tag{55}$$

By integration Eq. (55) and comparing with Eq. (47), Γ can be obtained as

$$\Gamma=-\Delta_{1t}(\kappa\Delta_{2t}-\overline{\kappa\Delta_{1t}})-2\Delta_{3t}(\kappa\Delta_{4t}-\overline{\kappa\Delta_{3t}}). \tag{56}$$

As mentioned, $\psi_t'^{\infty}$ expresses the thermal stress function for a laminate with no hole, as a result, it only causes the laminate deformation and does not generate stress. Thus, to achieve the thermal stresses, $\psi_t'^{M}$ should be determined using Eqs. (51), (53) and (55) as presented in the equation

$$\psi_t'^{M}(\xi)=-(\kappa\Delta_{2t}-\overline{\kappa\Delta_{1t}})\xi^{-1}-(\kappa\Delta_{4t}-\overline{\kappa\Delta_{3t}})\xi^{-2}. \tag{57}$$

Therefore, the temperature stress function of $\psi_t^M(\zeta)$ can be obtained as Eq. (58) by integrating Eq. (57):

$$\psi_t^M(\xi) = [-\Delta_{1t}(\kappa\Delta_{2t} - \overline{\kappa\Delta_{1t}}) - 2\Delta_{3t} \times$$
$$\times(\kappa\Delta_{4t} - \overline{\kappa\Delta_{3t}})]\log\xi + [\Delta_{1t}(\kappa\Delta_{4t} -$$
$$- \overline{\kappa\Delta_{3t}})]\xi^{-1} - \frac{1}{2}[\Delta_{2t}(\kappa\Delta_{2t} - \overline{\kappa\Delta_{1t}})]\xi^{-2} -$$
$$- \frac{1}{3}[\Delta_{2t}(\kappa\Delta_{4t} - \overline{\kappa\Delta_{3t}}) + 2\Delta_{4t}(\kappa\Delta_{2t} -$$
$$- \overline{\kappa\Delta_{1t}})]\xi^{-3} - [2\Delta_{3t}(\kappa\Delta_{2t} - \overline{\kappa\Delta_{1t}})] -$$
$$- \frac{1}{4}[2\Delta_{4t}(\kappa\Delta_{4t} - \overline{\kappa\Delta_{3t}})]\xi^4. \quad (58)$$

Finally, by comparing Eqs. (58) and (47), the functions $F_t(\xi)$ and $G_t(\xi)$ are obtained and by inserting them into Eq. (49), the complex analytical function of $\psi(\xi)$ can be achieved. Then, the stress components are obtained using Eq. (34).

5. Validation of the analytical solution

In order to validate the analytical results, ABAQUS/standard finite element code was used. Three dimensional finite element models were developed for the perforated composite laminates. The perforated laminates were considered considerably larger than the holes. Four-noded quadrilateral elements (S4R) were used for modeling composite laminates. A mesh sensitivity study was carried out and an acceptable number of elements were considered. According to Fig. 4, the region around the hole was modeled with fine mesh in order to capture the stress concentration. In this region, the number of elements was increased from 40 to 360 and it was observed that further increasing the number of elements did not change the results. Figure 5 compares the analytical and numerical circumferential stress σ_θ distributions around a quasi-triangular hole in the composite laminates made of different materials including graphite/epoxy (AS/3501) and E-glass/epoxy with different stacking sequences containing the holes with different specifications. In Fig. 5, angle of θ specifies the angular position on the border of the hole with respect to the horizontal axis. It can be seen from Fig. 5 that the

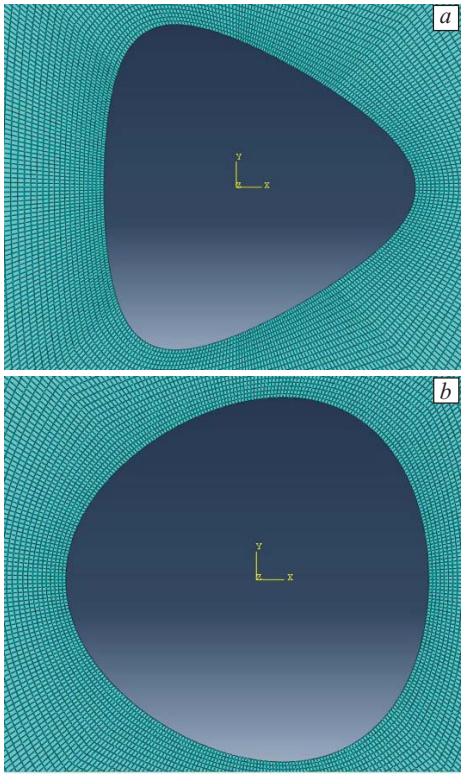

Fig. 4. Mesh refinement for composite laminate containing quasi-triangular hole. w = 0.10 (*a*), 0.05 (*b*), β = 0° (*a*), 60° (*b*)

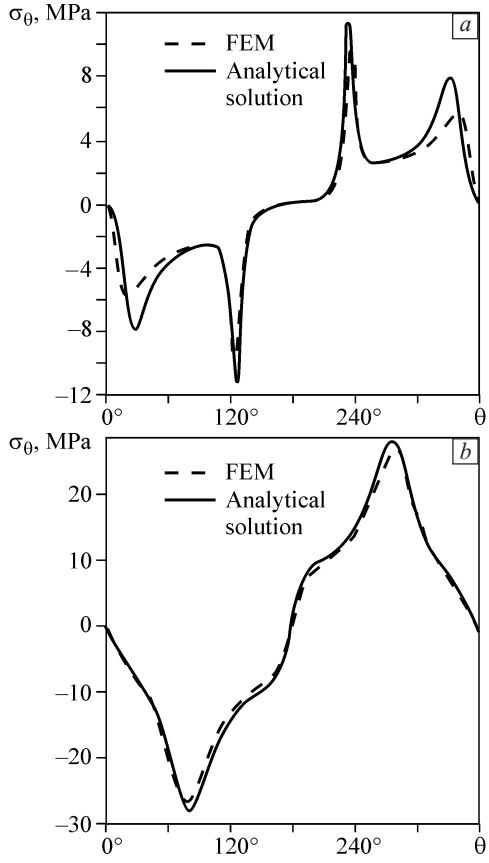

Fig. 5. Comparison between the finite element method (FEM) and the analytical results: graphite/epoxy (AS/3501) with $[45°/-45°]_s$ lay-up (*a*), E-glass/epoxy with $[0°/90°]_s$ lay-up (*b*); w = = 0.15 (*a*), 0.05 (*b*), β = 0° (*a*), 60° (*b*), c = 1, δ = 270°

Table 1

The material properties of the composite laminates

Material	E_{11}, GPa	E_{11}, GPa	G_{12}, GPa	v_{12}	α_{11}, K^{-1}	α_{22}, K^{-1}	K_{11}, $W m^{-1} K^{-1}$	K_{22}, $W m^{-1} K^{-1}$
Graphite/epoxy (AS/3501)	144.80	9.70	4.1	0.30	$-3.0 \cdot 10^{-6}$	$2.8 \cdot 10^{-5}$	4.62	0.72
E-glass/epoxy	35.00	9.00	4.7	0.28	$5.5 \cdot 10^{-6}$	$2.5 \cdot 10^{-5}$	2.20	1.10
Carbon/epoxy woven	91.82	91.82	19.5	0.05	$2.5 \cdot 10^{-6}$	$2.5 \cdot 10^{-6}$	3.50	2.60
Carbon/epoxy unidirectional	200.00	9.45	5.5	0.27	$0.4 \cdot 10^{-6}$	$30 \cdot 10^{-6}$	0.70	1.21

$E_{33} = E_{22}$, $G_{12} = G_{13} = G_{23}$, $v_{12} = v_{13} = v_{23}$, $\alpha_{33} = \alpha_{22}$, $K_{33} = K_{22}$, $K_{12} = 0$.

analytical results correlated reasonably well with the finite element method results.

6. Results and discussion

In this study, thermal stresses in symmetric laminated composites containing quasi-triangular hole were investigated. The distribution of thermal stress surrounding the hole was examined in terms of various parameters including the hole corner bluntness w, the hole aspect ratio c, the hole rotation angle β, the heat flux angle δ and the stacking sequence of laminated composite made of different materials. The mechanical properties of the laminates are listed in Table 1. In order to represent the effect of different parameters on the thermal stress distribution around the hole, the normalized maximum thermal stress was defined as

Table 2

Normalized thermal stress of each lamina in $[45°/–45°]_s$ laminate of different composite material in $w = 0.1$

θ	Graphite/epoxy (AS/3501)		E-glass/epoxy		Carbon/epoxy woven		Unidirectional carbon/epoxy	
	First layer	Second layer	First layer	Second layer	First layer	Second layer	First layer	Second layer
0°	0.0001	0.0001	0.0001	0.0001	0.0001	0.0001	0.0001	0.0001
5°	–0.0497	–0.0848	–0.1259	–0.1806	–0.1583	–0.1583	–0.0492	–0.0859
10°	–0.0799	–0.2318	–0.2096	–0.4190	–0.3257	–0.3257	–0.0773	–0.2360
20°	–0.1151	–0.8930	–0.2991	–0.9673	–0.6619	–0.6619	–0.1005	–0.9154
30°	–0.1391	–1.9756	–0.3350	–1.3146	–0.8669	–0.8669	–0.1041	–2.0372
40°	–0.1453	–2.0465	–0.3506	–1.3727	–0.9056	–0.9056	–0.1091	–2.1102
50°	–0.1440	–1.4948	–0.3644	–1.3055	–0.8751	–0.8751	–0.1184	–1.5361
60°	–0.1483	–1.0796	–0.3871	–1.2211	–0.8400	–0.8400	–0.1309	–1.1062
70°	–0.1618	–0.8138	–0.4276	–1.1474	–0.8198	–0.8198	–0.1498	–0.8316
80°	–0.1892	–0.6297	–0.4984	–1.0783	–0.8177	–0.8177	–0.1814	–0.6416
85°	–0.2114	–0.5554	–0.5517	–1.0399	–0.8240	–0.8240	–0.2055	–0.5648
90°	–0.2427	–0.4892	–0.6229	–0.9957	–0.8367	–0.8367	–0.2388	–0.4962
95°	–0.2879	–0.4296	–0.7191	–0.9436	–0.8584	–0.8584	–0.2863	–0.4342
100°	–0.3558	–0.3758	–0.8503	–0.8827	–0.8942	–0.8942	–0.3569	–0.3777
110°	–0.6451	–0.2853	–1.2689	–0.7381	–1.0381	–1.0381	–0.6551	–0.2794
120°	–1.6195	–0.2225	–1.8317	–0.5807	–1.2600	–1.2600	–1.6593	–0.1963
130°	–2.6372	–0.1776	–1.6827	–0.4240	–1.1075	–1.1075	–2.7212	–0.1307
140°	–0.7456	–0.1092	–0.8793	–0.2861	–0.6084	–0.6084	–0.7636	–0.0974
150°	–0.2297	–0.0702	–0.3961	–0.1849	–0.3013	–0.3013	–0.2340	–0.0674
160°	–0.0866	–0.0436	–0.1770	–0.1119	–0.1494	–0.1494	–0.0878	–0.0430
170°	–0.0301	–0.0220	–0.0675	–0.0545	–0.0629	–0.0629	–0.0304	–0.0219
180°	0.0001	0.0001	0.0001	0.0001	0.0001	0.0001	0.0001	0.0001

$$\sigma_{\text{norm}} = \frac{\sigma_{\theta,\max} k_x}{A(1,1)\, q_0 \lambda\, |\alpha_x|},$$

in which $\sigma_{\theta,\max}$ is the maximum circumferential stress induced around the hole. The effect of various geometrical and material parameters of the perforated composite laminate on the pick thermal stress value induced around the quasi-triangular hole was studied analytically. Among the studied cases in each section, the minimum value of the pick normalized thermal stress around the hole achieved by changing the parameters is called the desirable thermal stress and the maximum value of the pick normalized thermal stress is called undesirable thermal stress.

The thermal stresses induced in different layers of composite laminates made of graphite/epoxy (AS/3501), E-glass/epoxy, carbon/epoxy woven and unidirectional carbon/epoxy were determined. The stacking sequences considered for the laminates were $[45°/–45°]_s$ and $[0°/90°]_s$. Table 2 presents the normalized thermal stress values of different layers of the laminate with a stacking sequence of $[45°/–45°]_s$ and made of different materials. According to Table 2 and Fig. 6, the maximum thermal stress for the 45° layer of the graphite/epoxy (AS/3501) composite laminate was obtained at θ = 128° and 325° with the values of –2.8583 and 2.1802, respectively. Moreover, for the –45° layer, the maximum thermal stress values were obtained as –0.1446 and 0.1909 at θ = 35° and 232°, respectively. It is obvious that by changing the geometrical and material parameters, the thermal stress values were changed.

Table 3 presents the normalized thermal stress values induced in different layers of the composite laminate with a stacking sequence of $[0°/90°]_s$ and made of different materials. According to Table 3 and Fig. 6, the maximum thermal stresses for the 0° and 90° layers of the E-glass/epoxy composite laminate were obtained at θ = 257° and 233° with the values of 1.76004 and 0.5216, respectively. Figure 6 demonstrates the normalized thermal stress distributions in different layers of the composite laminates made of graphite/epoxy (AS/3501) and E-glass/epoxy and with the stacking sequences of $[45°/–45°]_s$ and $[0°/90°]_s$ around a quasi-triangular hole.

6.1. The effect of hole aspect ratio

In this section, for studying the effect of hole aspect ratio c on the maximum thermal stress around the hole, the flux angle, the bluntness and the rotation angle of the hole were cosidered δ = 270°, w = = 0.05 and β = 0°, respectively. Figure 7 illustrates the effect of c parameter on the shape of the quasi-triangular hole. The effect of hole aspect ratio on the normalized maximum thermal stress value around the quasi-triangular hole in the perforated composite laminate is shown in Table 4. It is observed for the stacking sequence of $[45°/–45°]_s$ that the desirable and undesirable thermal stresses were achieved at c = 1 and 2.5, respectively. It can be seen in Table 4 that the thermal stress value around the hole is considerably dependent on the hole aspect ratio. It can be seen that the thermal stress around the hole, initially decreased from c = 0.5 to 1.0 and further increase of c resulted in increase of thermal stress. However, for the stacking sequence of $[0°/90°]_s$, the thermal stress value continuously increased by increasing the parameter c.

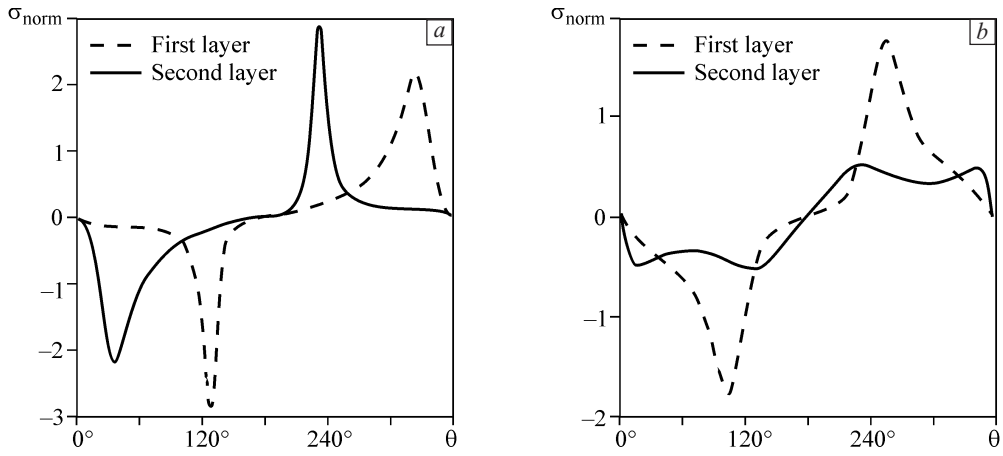

Fig. 6. Thermal stress distribution for the first and second layers of composite laminates: graphite/epoxy (AS/3501) laminate of $[45°/–45°]_s$ stacking (*a*), E-glass/epoxy laminate of $[0°/90°]_s$ stacking (*b*)

Table 3

Normalized thermal stress of each lamina in $[0°/90°]_s$ laminate of different composite material in $w = 0.1$

θ	Graphite/epoxy (AS/3501)		E-glass/epoxy		Carbon/epoxy woven		Unidirectional carbon/epoxy	
	First layer	Second layer	First layer	Second layer	First layer	Second layer	First layer	Second layer
0°	0.0001	0.0001	0.0001	0.0001	0.0001	0.0001	0.0001	0.0001
5°	–0.0222	–0.2487	–0.0747	–0.2740	–0.1758	–0.1758	–0.0177	–0.2526
10°	–0.0411	–0.2614	–0.1451	–0.4326	–0.2896	–0.2896	–0.0366	–0.2642
20°	–0.0767	–0.1851	–0.2673	–0.4785	–0.3709	–0.3709	–0.0740	–0.1858
30°	–0.1115	–0.1398	–0.3660	–0.4270	–0.3933	–0.3933	–0.1100	–0.1391
40°	–0.1475	–0.1158	–0.4493	–0.3810	–0.4119	–0.4119	–0.1469	–0.1142
50°	–0.1899	–0.1032	–0.5315	–0.3527	–0.4391	–0.4391	–0.1900	–0.1006
60°	–0.2490	–0.0973	–0.6312	–0.3403	–0.4834	–0.4834	–0.2501	–0.0936
70°	–0.3488	–0.0967	–0.7743	–0.3423	–0.5570	–0.5570	–0.3512	–0.0910
80°	–0.5538	–0.1012	–0.9998	–0.3581	–0.6799	–0.6799	–0.5593	–0.0916
85°	–0.7490	–0.1060	–1.1583	–0.3716	–0.7678	–0.7678	–0.7578	–0.0928
90°	–1.0696	–0.1133	–1.3493	–0.3887	–0.8747	–0.8747	–1.0846	–0.0941
95°	–1.5647	–0.1240	–1.5551	–0.4092	–0.9912	–0.9912	–1.5913	–0.0954
100°	–2.0345	–0.1353	–1.7199	–0.4320	–1.0875	–1.0875	–2.0737	–0.0978
110°	–1.1446	–0.1374	–1.5823	–0.4763	–1.0349	–1.0349	–1.1595	–0.1169
120°	–0.3736	–0.1460	–0.9469	–0.5105	–0.7251	–0.7251	–0.3751	–0.1404
130°	–0.1485	–0.1668	–0.4804	–0.5200	–0.4962	–0.4962	–0.1469	–0.1658
140°	–0.0706	–0.1915	–0.2474	–0.4755	–0.3598	–0.3598	–0.0676	–0.1923
150°	–0.0373	–0.2084	–0.1322	–0.3723	–0.2527	–0.2527	–0.0338	–0.2105
160°	–0.0203	–0.1950	–0.0695	–0.2427	–0.1572	–0.1572	–0.0168	–0.1978
170°	–0.0092	–0.1244	–0.0301	–0.1167	–0.0741	–0.0741	–0.0069	–0.1267
180°	0.0001	0.0001	0.0001	0.0001	0.0001	0.0001	0.0001	0.0001

For the stacking sequence of $[0°/90°]_s$, the lowest value of the maximum thermal stress was obtained for the graphite/epoxy (AS/3501) material and the highest value was obtained for the carbon/epoxy woven material. Figure 8 shows the effect of hole aspect ratio c on the variation of normalized thermal stress and composite materials behavior in the laminates containing quasi-triangular hole for two stacking sequence of $[45°/–45°]_s$ and $[0°/90°]_s$. According to Fig. 8, for the stacking sequence of $[45°/–45°]_s$, the desirable stresses achieved for the graphite/epoxy (AS/3501), E-glass/epoxy, carbon/epoxy woven and unidirectional carbon/epoxy materials were in the range of $0.5 \le c \le 1$.

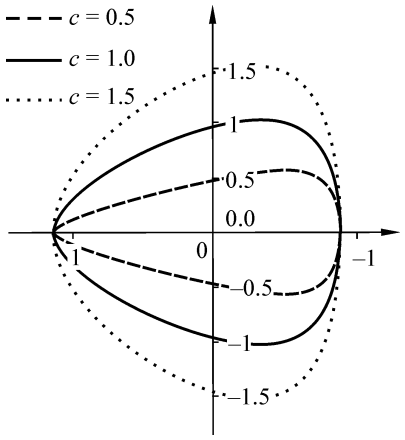

Fig. 7. The effect of c on the shape of quasi-triangular hole

6.2. The effect of hole rotation angle

The effect of rotation angle parameter β on the normalized thermal stress distribution around the quasi-triangular hole for the stacking sequences of $[45°/–45°]_s$ and $[0°/90°]_s$ was studied. The effect of β on the perforated composite laminates with different materials and stacking sequences are presented in Table 5. In this section, for studying the effect of

Table 4

The normalized maximum thermal stress value in symmetric laminates for different hole aspect ratios

Stacking sequence	Graphite/epoxy (AS/3501)		E-glass/epoxy		Carbon/epoxy woven		Unidirectional carbon/epoxy	
	c	σ_{norm}	c	σ_{norm}	c	σ_{norm}	c	σ_{norm}
$[45°/–45°]_s$	0.5	1.6606	0.5	1.2262	0.5	1.2894	0.5	1.6827
	1.0	1.3693	1.0	1.0896	1.0	1.1421	1.0	1.3873
	1.5	1.4814	1.5	1.2238	1.5	1.2809	1.5	1.5009
	2.0	1.6493	2.0	1.3982	2.0	1.4616	2.0	1.6710
	2.5	1.8441	2.5	1.5881	2.5	1.6581	2.5	1.8676
$[0°/90°]_s$	0.5	0.7965	0.5	0.8130	0.5	0.8204	0.5	0.7970
	1.0	1.0247	1.0	1.0180	1.0	1.0287	1.0	1.0255
	1.5	1.2682	1.5	1.2555	1.5	1.2689	1.5	1.2693
	2.0	1.5150	2.0	1.4979	2.0	1.5140	2.0	1.5163
	2.5	1.7559	2.5	1.7416	2.5	1.7601	2.5	1.7573

the rotation angle, it was assumed that $\delta = 270°$, $w = 0.05$ and $c = 1$. It is observed that for the stacking sequence of $[45°/–45°]_s$ the desirable thermal stress was achieved at a rotation angle of $\beta = 30°$. The desirable thermal stresses obtained at $\beta = 30°$ for different materials of graphite/epoxy (AS/3501), E-glass/

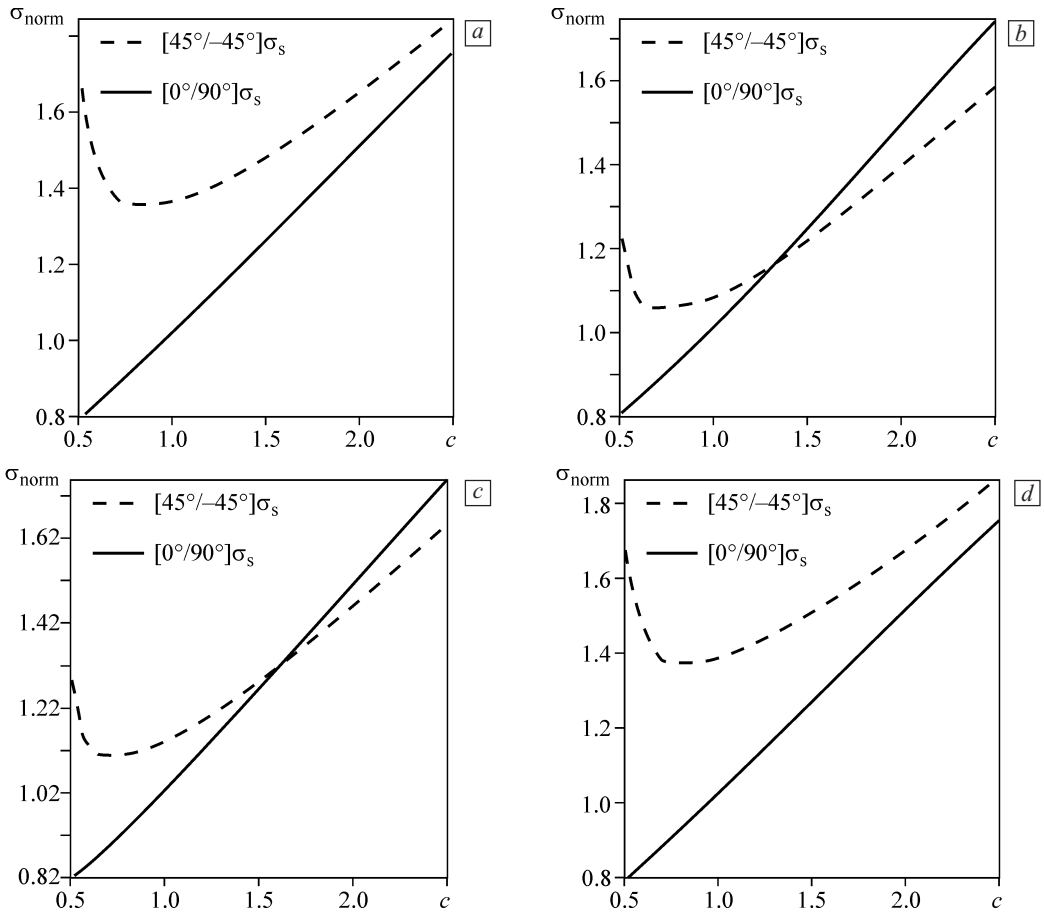

Fig. 8. Effect of the hole aspect ratio on σ_{norm} for different composite materials and stacking sequences: graphite/epoxy (AS/3501) (*a*), E-glass/epoxy (*b*), carbon/epoxy woven (*c*), unidirectional carbon/epoxy (*d*)

Table 5

Normalized thermal stress values for different rotation angles of hole

Stacking sequence	Graphite/epoxy (AS/3501)		E-glass/epoxy		Carbon/epoxy woven		Unidirectional carbon/epoxy	
	β	σ_{norm}	β	σ_{norm}	β	σ_{norm}	β	σ_{norm}
$[45°/–45°]_s$	0°	1.3693	0°	1.0896	0°	1.1421	0°	1.3873
	30°	1.1986	30°	0.9897	30°	1.0351	30°	1.2143
	45°	1.2944	45°	1.0553	45°	1.1047	45°	1.3113
	60°	1.3693	60°	1.0896	60°	1.1421	60°	1.3873
	90°	1.3548	90°	1.0399	90°	1.0918	90°	1.3726
$[0°/90°]_s$	0°	1.0247	0°	1.0180	0°	1.0287	0°	1.0255
	30°	1.1095	30°	1.0965	30°	1.1083	30°	1.1105
	45°	1.086	45°	1.0754	45°	1.0869	45°	1.0869
	60°	1.0247	60°	1.0180	60°	1.0287	60°	1.0255
	90°	0.9078	90°	0.8972	90°	0.9068	90°	0.9086

epoxy, carbon/epoxy woven and unidirectional carbon/epoxy having the stacking sequence of $[45°/–45°]_s$ were 1.1986, 0.9897, 1.0351 and 1.2143, respectively. However, for the stacking sequence of $[0°/90°]_s$ the desirable thermal stress was obtained at the rotation angle of β = 90°. Moreover, for the stacking se-

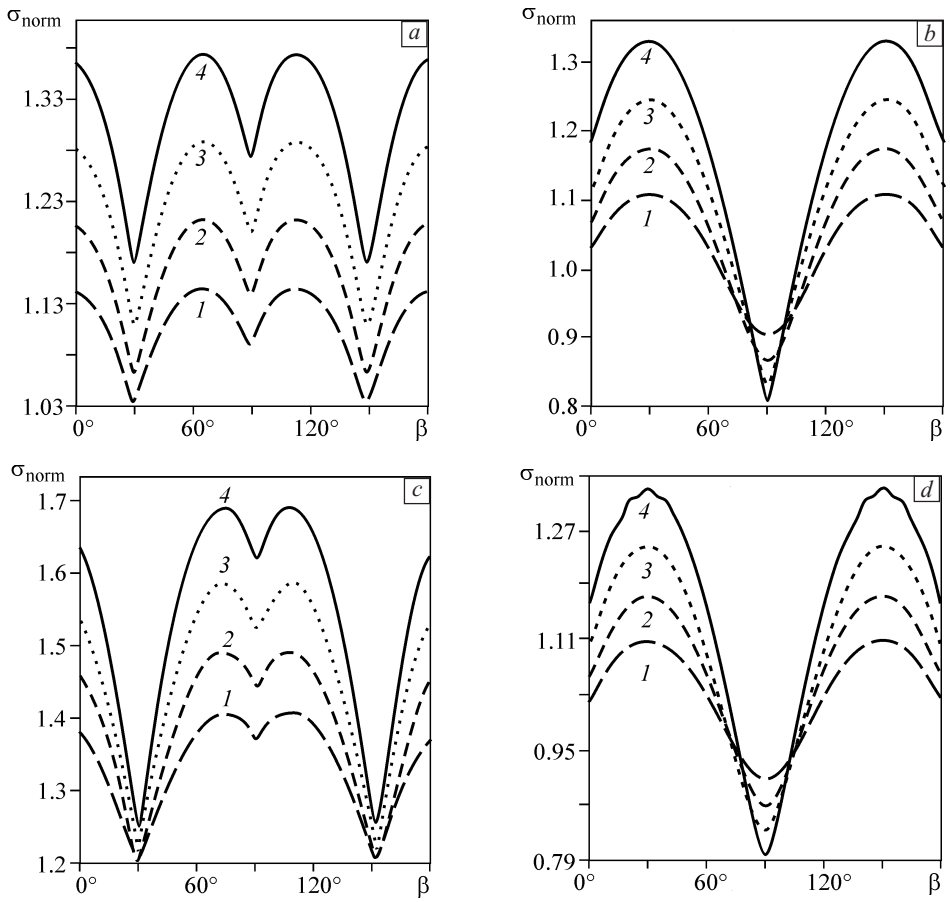

Fig. 9. Effect of the hole rotation angle on the normalized thermal stress for different values of *w*: 0.050 (*1*), 0.075 (*2*), 0.100 (*3*), 0.125 (*4*); $[45°/–45°]_s$ (*a*, *c*), $[0°/90°]_s$ (*b*, *d*)

Table 6

Normalized thermal stress values for different heat flux angles

Stacking sequence	Graphite/epoxy (AS/3501)		E-glass/epoxy		Carbon/epoxy woven		Unidirectional carbon/epoxy	
	δ	σ_{norm}	δ	σ_{norm}	δ	σ_{norm}	δ	σ_{norm}
$[45°/–45°]_s$	0°	1.1986	0°	0.9897	0°	1.0351	0°	1.2143
	30°	1.6061	30°	1.2106	30°	1.2716	30°	1.6274
	45°	1.6575	45°	1.2287	45°	1.2917	45°	1.6796
	60°	1.5989	60°	1.1786	60°	1.2394	60°	1.6202
	90°	1.3693	90°	1.0896	90°	1.1421	90°	1.3873
$[0°/90°]_s$	0°	1.1095	0°	1.0965	0°	1.1083	0°	1.1105
	30°	0.9646	30°	0.9731	30°	0.9825	30°	0.9653
	45°	0.7952	45°	0.8312	45°	0.8383	45°	0.7958
	60°	0.8873	60°	0.8817	60°	0.8910	60°	0.8880
	90°	1.0247	90°	1.0180	90°	1.0287	90°	1.0255

quence of $[0°/90°]_s$, the minimum normalized thermal stress was obtained for the E-glass/epoxy material with the value of 0.8972 and the maximum normalized thermal stress was obtained for the unidirectional carbon/epoxy material with the value of 1.1105. The variations of the normalized thermal stress with the hole rotation angle for different values of the hole bluntness and the stacking sequences of $[45°/–45°]_s$ and $[0°/90°]_s$ for the carbon/epoxy woven and the unidirectional carbon/epoxy materials are shown in Fig. 9.

6.3. The effect of heat flux angle

Table 6 presents the influence of the heat flux angle δ on the normalized thermal stress value around the quasi-triangular hole in a four-layer symmetric composite laminate made of different materials with two stacking sequences. It was assumed that the heat flux angle was varied between 0° and 90° and its effect on the normalized thermal stress was studied. It was found out that the effect of δ on the normalized thermal stress value for the two stacking sequences of $[45°/–45°]_s$ and $[0°/90°]_s$ were different. According to Table 6, the minimum and maximum normalized thermal stress values were obtained for δ = 0° and 45° for the stacking sequence of $[45°/–45°]_s$, respectively. While, for the stacking sequence of $[0°/90°]_s$ the minimum and maximum thermal stress values were obtained for δ = 45° and 0°, respectively.

For the stacking sequence of $[0°/90°]_s$, the desirable normalized thermal stress values obtained for the graphite/epoxy (AS/3501), E-glass/epoxy, carbon/epoxy woven and unidirectional carbon/epoxy materials were equal to 0.7952, 0.8312, 0.8383 and 0.7958, respectively. In order to better observe the heat flux angle effect on the normalized thermal stress for dif-

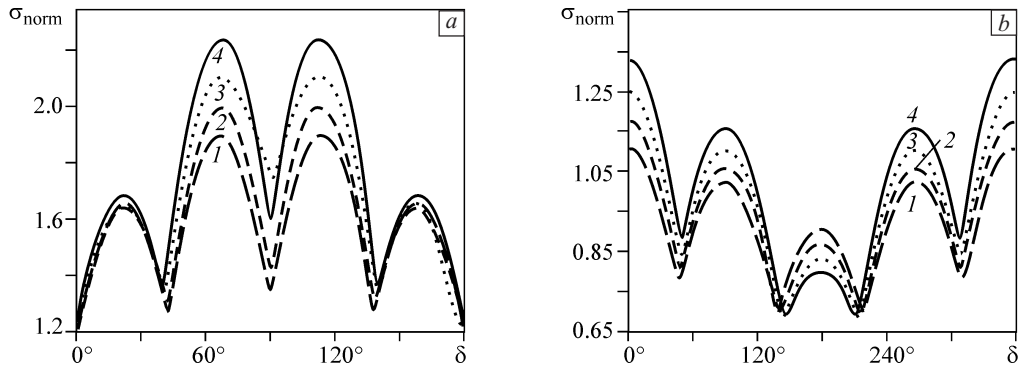

Fig. 10. Effect of heat flux angle on σ_{norm} for the laminate made of graphite/epoxy (AS/3501) for different values of *w*: 0.050 (*1*), 0.075 (*2*), 0.100 (*3*), 0.125 (*4*); $[45°/–45°]_s$ (*a*), $[0°/90°]_s$ (*b*)

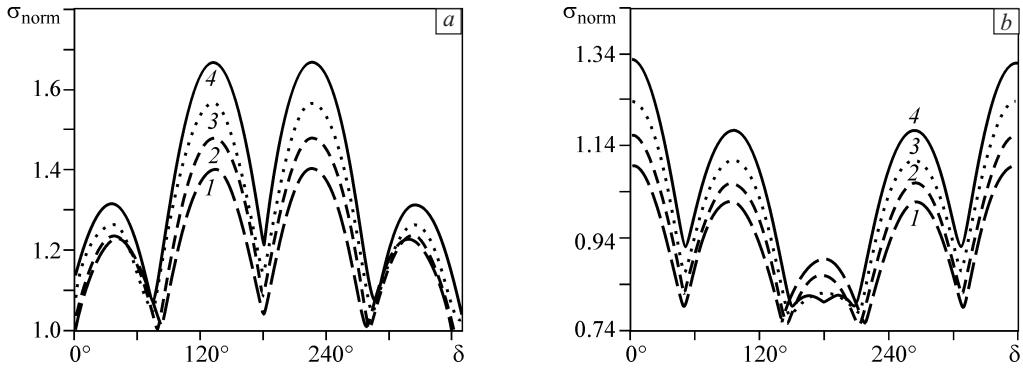

Fig. 11. Effect of heat flux angle on σ_{norm} for the E-glass/epoxy and different values of w: 0.050 (*1*), 0.075 (*2*), 0.100 (*3*), 0.125 (*4*); [45°/–45°]$_s$ (*a*), [0°/90°]$_s$ (*b*)

ferent values of the hole bluntness, Figs. 10 and 11 are presented. As observed in Fig. 10, by increasing the value of w and the sharpening the hole corners, both of the desirable and undesirable thermal stresses were increased. For the graphite/epoxy (AS/3501) material with the stacking sequence of [45°/–45°]$_s$, for all values of w, the desirable normalized thermal stress occurred at the angles of approximately 70° and 280°. Whereas, for the stacking sequence of [0°/90°]$_s$, the desirable normalized thermal stress occurred at the angles of approximately 145° and 215°.

Moreover, it is clear in Fig. 11 that for the glass/epoxy material with the stacking sequence of [45°/–45°]$_s$ for all values of w, the desirable normalized thermal stress occurred at the angles of approximately 80° and 280°. Wherase, for the stacking sequence of [0°/90°]$_s$, the desirable normalized thermal stress occurred at the angles of approximately 145° and 215°. It should be noted that the results of Table 6 are presented with the assumptions of $\beta = 0°$, $w = 0.05$ and $c = 1$.

6.4. The effect of bluntness

Table 7 represents the effect of the hole corner bluntness w on the normalized thermal stress. It can be seen in Table 7 that the thermal stress value in-

Table 7

Normalized thermal stress for different bluntness values

Stacking sequence	Graphite/epoxy (AS/3501)		E-glass/epoxy		Carbon/epoxy woven		Unidirectional carbon/epoxy	
	w	σ_{norm}	w	σ_{norm}	w	σ_{norm}	w	σ_{norm}
[45°/–45°]$_s$	0	1.252	0	0. 9831	0	1.031	0	1.2685
	0.05	1.3693	0.05	1.0896	0.05	1.1421	0.05	1.3873
	0.10	1.5247	0.10	1.2243	0.10	1.2833	0.10	1.5449
	0.15	1.7385	0.15	1.3990	0.15	1.4956	0.15	1.7615
	0.20	2.0137	0.20	1.6292	0.20	1.7080	0.20	2.0394
	0.25	2.4158	0.25	1.9579	0.25	2.0508	0.25	2.4467
	0.30	2.9758	0.30	2.4457	0.30	2.5639	0.30	3.0128
[0°/90°]$_s$	0.00	0.9986	0.00	0.9869	0.00	0.9975	0.00	0.9994
	0.05	1.0247	0.05	1.0180	0.05	1.0287	0.05	1.0255
	0.10	1.1006	0.10	1.1047	0.10	1.1159	0.10	1.1015
	0.15	1.2293	0.15	1.2423	0.15	1.2546	0.15	1.2302
	0.20	1.4225	0.20	1.4399	0.20	1.4540	0.20	1.4236
	0.25	1.7020	0.25	1.7238	0.25	1.7411	0.25	1.7032
	0.30	2.1305	0.30	2.1581	0.30	2.1796	0.30	2.1322

creased with increasing the hole bluntness. The minimum thermal stress value occurred when the bluntness parameter was zero ($w = 0$). As shown in Fig. 3, $w = 0$ is equivalent to a circular hole. Therefore, the thermal stress value in a perforated symmetric laminate with a circular hole was always lower compared to the quasi-triangular holes. For the stacking sequence of $[45°/–45°]_s$, the desirable thermal stress obtained at $w = 0$ for the E-glass/epoxy composite laminate with the value of 0.9831 and the undesirable thermal stress value obtained at $w = 0.3$ for the unidirectional carbon/epoxy composite laminate with the value of 3.0128. However, in the stacking sequence of $[0°/90°]_s$, the desirable thermal stress value obtained at $w = 0$ for the E-glass/epoxy composite laminate with the value of 0.9869 and the undesirable thermal stress value obtained at $w = 0.3$ for the carbon/epoxy woven composite laminate with the value of 2.1796. Figure 12 illustrates the variations of normalized thermal stress in the laminates containing quasi-triangular hole in terms of the bluntness parameter for two stacking sequences of $[45°/–45°]_s$ and $[0°/90°]_s$. It can be observed that the normalized thermal stress increased by increasing the bluntness parameter and yet the rate of this increase was steeper for the larger bluntness values. Furthermore, it is evident from Fig. 12 that the normalized stress in the stacking sequence of $[45°/–45°]_s$ was always higher than that of the stacking sequence of $[0°/90°]_s$ in all composite materials. Figure 13 shows the normalized thermal stress distribution in different perforated composite materials around the quasi-triangular hole with different values of w and β parameters. The results presented in this section were obtained by considering $\beta = 0°$, $\delta = 270°$ and $c = 1$.

7. Conclusions

The thermal stress distribution around the quasi-triangular hole in a symmetric laminated plate with various composite materials under a uniform heat flux

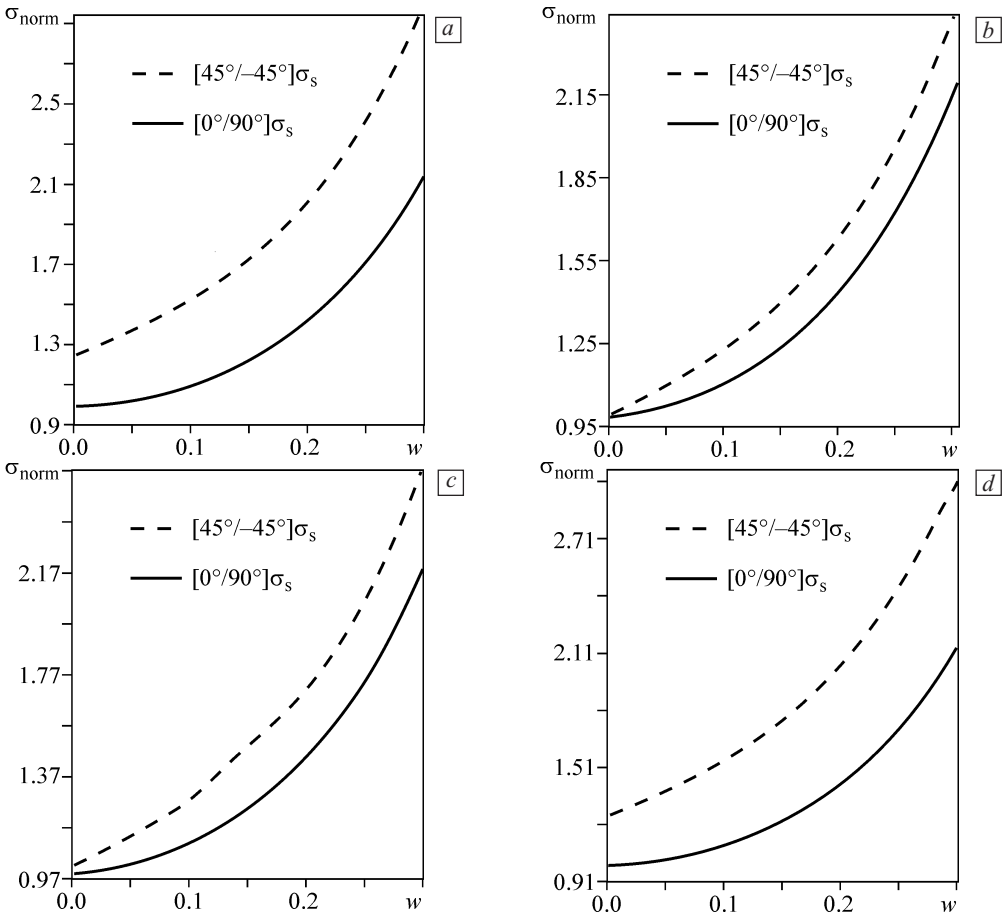

Fig. 12. Effect of bluntness on σ_{norm} for different composite materials and stacking sequences: graphite/epoxy (AS/3501) (*a*), E-glass/epoxy (*b*), carbon/epoxy woven (*c*), unidirectional carbon/epoxy (*d*)

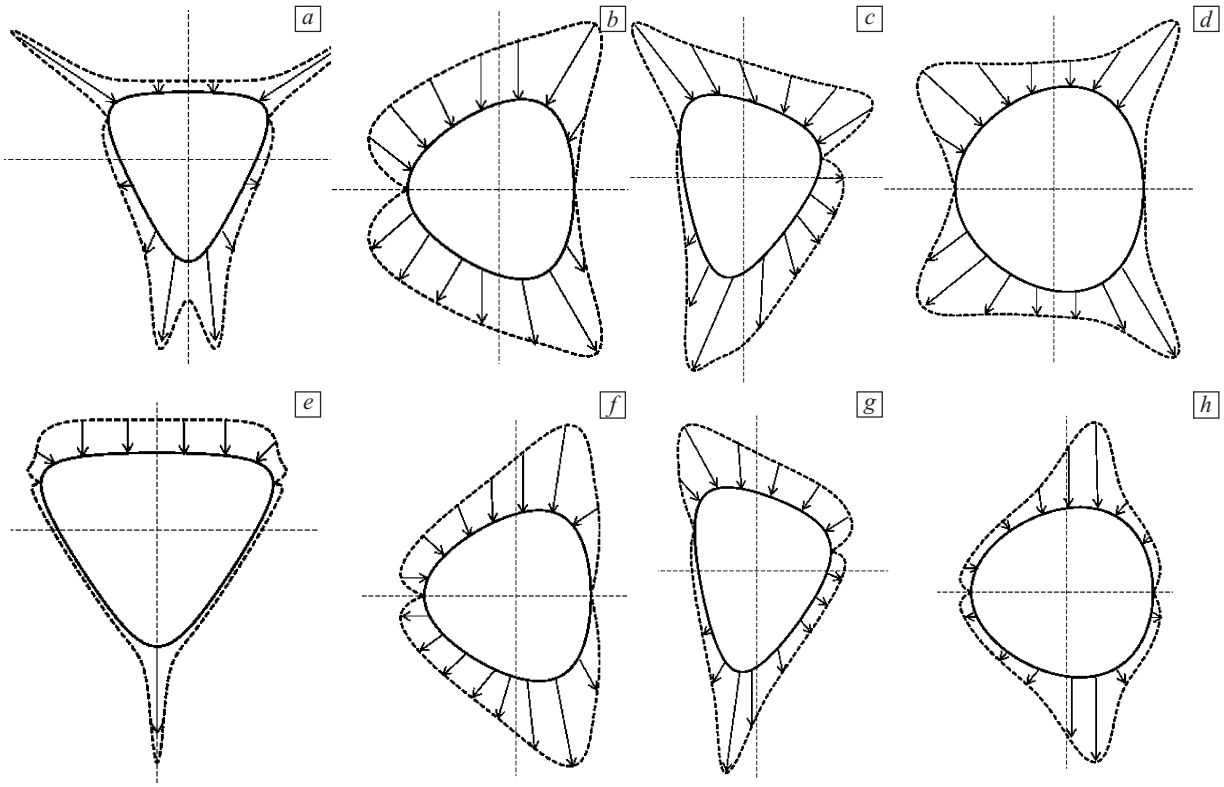

Fig. 13. Thermal stress distribution around the quasi-triangular hole with β = 30° (*a*, *e*), 0° (*b*, *d*, *f*, *h*), 45° (*c*, *g*); w = 0.2 (*a*, *e*), 0.1 (*b*, *f*), 0.15 (*c*, *g*), 0.05 (*d*, *h*); σ_{norm} = 1.465 (*a*), 1.5247 (*b*), 1.3895 (*c*), 1.0255 (*d*, *h*), 1.6643 (*e*), 1.1047 (*f*), 1.3807 (*g*). Graphite/epoxy (AS/3501) (*a*, *e*), E-glass/epoxy (*b*, *f*), carbon/epoxy woven (*c*, *g*), unidirectional carbon/epoxy (*d*, *h*). Stacking sequence of $[45°/–45°]_s$ (*a*–*d*), $[0°/90°]_s$ (*e*–*h*)

was studied analytically using the Lekhnitskii's complex variable technique and a conformal transferring function. It was assumed that the edges of the hole were thermally insulated and had Neumann boundary condition. The analytical method was validated with finite element results. The thermal stress distribution in each lamina for different composite materials was analyzed. Furthermore, the effects of the laminate stacking sequence, the heat flux angle and the hole bluntness, aspect ratio and rotation angle as important parameters and behavior of composite materials were investigated on the thermal stress distribution. It was found out that for the composite materials and the two stacking sequences of $[45°/–45°]_s$ and $[0°/90°]_s$ studied in this research, the minimum normalized thermal stress value was obtained for the circular hole (i.e. w = 0). Moreover, increasing the hole aspect ratio increased the thermal stress surrounding the quasi-triangular hole. The results showed that the hole orientation can influence the thermal stress value considerably. The hole rotation angles of 30° and 90° resulted minimum thermal stress values in the perforated laminates with stacking sequences of $[45°/–45°]_s$ and $[0°/90°]_s$, respectively. Moreover, it was found that applying the heat flux angles of 0° and 45° on the perforated laminates with the stacking sequences of $[45°/–45°]_s$ and $[0°/90°]_s$, respectively, caused lower thermal stress values around the hole.

References

1. *Muskhelishvili N.* Some Basic Problems of the Mathematical Theory of Elasticity. – Dordrecht: Springer Netherlands, 1954.
2. *Savin G.N.* Stress Distribution around Holes. – New York: 1961.
3. *Lekhnitskiy S.G.* Anisotropic Plates. – New York: Epub ahead of print, 1969. – doi 0677206704.
4. *Hasebe N., Wang X.* Complex variable method for thermal stress problem // J. Therm. Stress. – 2005. – V. 28. – P. 595–648.
5. *Florence A.L., Goodier J.N.* Thermal stresses due to disturbance of uniform heat flow by an insulated ovaloid hole // J. Appl. Mech. – 1960. – V. 27. – P. 635–639.
6. *Bhullar S.K., Wegner J.L.* Thermal stresses in a plate with hyperelliptical hole // J. Eng. Technol. Res. – 2009. – V. 1. – P. 152–170.

7. *Tarn J.Q., Wang Y.M.* Thermal stresses in anisotropic bodies with a hole or a rigid inclusion // J. Therm. Stress. – 1993. – V. 16. – P. 455–471.
8. *Chauhan M.M., Sharma D.S.* Stress concentration at the corners of polygonal hole in finite plate // Aerosp. Sci. Technol. – 2016. – V. 58. – P. 197–206.
9. *Kalyon M., Yilbas B.S.* Analytical solution for thermal stresses during the laser pulse heating process // Proc. Inst. Mech. Eng. Part C. J. Mech. Eng. Sci. – 2001. – V. 215. – P. 1429–1445.
10. *Su Z., Xie C., Tang Y.* Stress distribution analysis and optimization for composite laminate containing hole of different shapes // Aerosp. Sci. Technol. – 2018. – V. 76. – P. 466–470.
11. *Ju S.H., Liang W.Y., Hsu H.H., Tarn J.Q.* Analytic solution of angle-ply laminated plates under extension, bending and torsion // J. Compos. Mater. – 2019. – doi 10.1177/0021998319873025.
12. *Alshaya A., Lin S.* Hybrid stress analysis of a near-surface circular hole in finite structures // Proc. Inst. Mech. Eng. C. J. Mech. Eng. Sci. – 2019. – P. 1–16.
13. *Damghani M., Harrison C., Kennedy D.* The effects of composite laminate stiffness and loading on stress resultant concentration factor around a hole // Proc. Inst. Mech. Eng. Part C. J. Mech. Eng. Sci. – 2018. – V. 232. – P. 1033–1049.
14. *Khechai A., Mohite P.M.* Optimum design of perforated symmetric laminates using evolutionary algorithm // J. Compos. Mater. – 2019. – V. 53. – P. 3281–3305.
15. *Jafari M., Nazari M.B., Taherinasab A.* Thermal stress analysis in metallic plates with a noncircular hole subjected to uniform heat flux // Eur. J. Mech. A. Solids. – 2016. – V. 59. – P. 356–363.
16. *Jafari M., Jafari M.* Effect of hole geometry on the thermal stress analysis of perforated composite plate under uniform heat flux // J. Compos. Mater. – 2019. – V. 53. – P. 1079–1095.
17. *Choi H.J.* Thermal stresses due to a uniform heat flow disturbed by a pair of offset parallel cracks in an infinite plane with orthotropy // Eur. J. Mech. A. Solids. – 2017. – V. 63. – P. 1–13.
18. *Mahmoudi H., Atefi G.* Analytical solution for thermal stresses in a hollow cylinder under periodic thermal loading // Proc. Inst. Mech. Eng. Part C. J. Mech. Eng. Sci. – 2012. – V. 226. – P. 1705–1724.
19. *Chao C.K., Chen F.M., Lin T.H.* Thermal stresses induced by a remote uniform heat flow interacting with two circular inclusions // J. Therm. Stress. – 2017. – V. 40. – P. 564–582.
20. *Wang P., Wang B.L.* Thermoelectric fields and associated thermal stresses for an inclined elliptic hole in thermoelectric materials // Int. J. Eng. Sci. – 2017. – V. 119. – P. 93–108.
21. *Zenkour A.M., Abouelregal A.E.* Thermoelastic interactions in an infinite orthotropic continuum of a variable thermal conductivity with a cylindrical hole // Iran. J. Sci. Technol. Trans. Mech. Eng. – 2019. – V. 43. – P. 281–290.
22. *Ukadgaonker V.G., Rao D.K.N.* A general solution for stresses around holes in symmetric laminates under in-plane loading // Compos. Struct. – 2000. – V. 49. – P. 339–354.
23. *Zha X., Zuo Y.* Theoretical and experimental studies on in-plane stiffness of integrated container structure // Adv. Mech. Eng. – 2016. – V. 8. – P. 1–20.
24. *Dehghani M., Fotuhi A.R., Shafiei A.R.* Thermal stress analysis in a finite perforated plane // Iran. J. Sci. Technol. Trans. Mech. Eng. – 2019. – V. 43. – P. 705–721.
25. *Khoramishad H., Bagheri Tofighi M., Khodaei M.* Effect of Stacking Sequence on Low-Velocity Impact Behavior of Metal Laminates // Phys. Mesomech. – 2018. – V. 21. – No. 2. – P. 140–149. – doi 10.1134/S1029959918020078.
26. *Herakovich C.T.* Mechanics of Fibrous Composites. – Virginia: Johan Wiley and Sons, 1998.
27. *Ozisik N.M.* Heat Conduction. – New York: John Wiley and Sons, 1993.
28. *Jafari M., Moussavian H., Bayati M.H.C.* Optimum design of perforated orthotropic and laminated composite plates under in-plane loading by genetic algorithm // Struct. Multidiscip. Optim. – 2018. – V. 57. – P. 341–357.
29. *Chao C.K., Shen M.H.* Thermal stresses in a generally anisotropic body with an elliptic inclusion subject to uniform heat flow // J. Appl. Mech. – 1998. – P. 51–65.

Received 22.01.2020,
revised 22.01.2020,
accepted 29.01.2020

Сведения об авторах

Mohammad Hossein Bayati Chaleshtari, PhD Candidate, School of Mechanical Engineering, Iran University of Science and Technology, Iran, bayati_m@mecheng.iust.ac.ir
Hadi Khoramishad, PhD, Assoc. Prof., School of Mechanical Engineering, Iran University of Science and Technology, Iran, Khoramishad@iust.ac.ir
Filippo Berto, Prof., Norwegian University of Science and Technology, Norway, filippo.berto@ntnu.no